

## MULTI-DIMENSIONAL DOUBLE DETONATION OF SUB-CHANDRASEKHAR MASS WHITE DWARFS

R. MOLL AND S. E. WOOSLEY

Department of Astronomy and Astrophysics, University of California, Santa Cruz, CA 95064, USA

(Dated: March 5, 2013)

## ABSTRACT

Using 2D and 3D simulation, we study the “robustness” of the double detonation scenario for Type Ia supernovae, in which a detonation in the helium shell of a carbon-oxygen white dwarf induces a secondary detonation in the underlying core. We find that a helium detonation cannot easily descend into the core unless it commences (artificially) well above the hottest layer calculated for the helium shell in current presupernova models. Compressional waves induced by the sliding helium detonation, however, robustly generate hot spots which trigger a detonation in the core. Our simulations show that this is true even for non-axisymmetric initial conditions. If the helium is ignited at multiple points, the internal waves can pass through one another or be reflected, but this added complexity does not defeat the generation of the hot spot. The ignition of very low-mass helium shells depends on whether a thermonuclear runaway can simultaneously commence in a sufficiently large region.

*Subject headings:* hydrodynamics – nuclear reactions, nucleosynthesis, abundances – shock waves – supernovae: general – white dwarfs

## 1. INTRODUCTION

In the double detonation scenario, a carbon-oxygen (CO) white dwarf accumulates a layer of helium through accretion from a helium main sequence star. The accretion rate, typically on the order of  $10^{-8}$ – $10^{-7} M_{\odot} \text{ yr}^{-1}$  (e.g., Taam 1980; Woosley & Weaver 1994), and the mass of the white dwarf determine the critical thickness of the helium layer. Generally, a low accretion rate allows more helium to accumulate before a thermonuclear runaway commences near the base of the helium shell, the temperature of which is determined by gravitational compression, convection and eventually nuclear burning. It is often assumed that a detonation in the helium induces a secondary detonation in the CO core, thus producing a Type Ia supernova.

If and how a secondary core detonation develops is ambiguous, however. One possibility is that the core is ignited directly at the core-shell interface when hit by the helium detonation front. This is sometimes called “direct drive”, “edge-lit scenario” or “prompt detonation”. It has long been realized that this does not always work and that its realization depends on the altitude at which the helium detonation starts (e.g., Livne & Glasner 1990; Benz 1997; García-Senz et al. 1999). A helium detonation directly at the interface almost certainly fails to start a detonation in the core, but evolution models of accreting white dwarfs suggest that the most probable place for a detonation to start could be higher up (Woosley & Kasen 2011). One of the aims of the present work is to determine whether a helium detonation ignited at a point in the hottest helium layer would lead to core detonation by direct drive.

If direct drive fails, the core may still ignite, with considerable delay, after the detonation wave has consumed the entire helium layer, through compressional waves which focus inside the core. In the simplest (and most unrealistic) scenario, the star is spherically symmetric and the helium is ignited instantaneously in a spherical shell. This induces a radially inward propagating compressional wave that converges at the exact center of the

star, where, depending upon the resolution of the study, it always ignites the core (e.g., Livne 1990).

Since convective mixing is not able to keep the temperature at a given radius constant before the runaway, it is more likely that helium ignition starts in one or more isolated regions with sizes of perhaps a pressure scale height (Woosley & Kasen 2011). If the detonation starts at a single point, the sliding helium detonation creates an oblique (with respect to the core-shell interface) shock wave that converges inside the core at the axis of symmetry and potentially triggers an off-center core detonation (Dgani & Livio 1990; Livne & Glasner 1990, 1991; Livne & Arnett 1995). In their simulations of double-detonation supernovae, Fink et al. (2007) considered a variety of 1D and 2D helium ignition scenarios, confirming the high ignition potential of the inward propagating shock wave. They showed that core detonation resulting from the detonation of the helium in a single spot is very likely even for low mass helium shells, for instance  $0.0035 M_{\odot}$  in combination with a  $1.3850 M_{\odot}$  core (Fink et al. 2010), and for core masses as low as  $0.45 M_{\odot}$  (Sim et al. 2012).

In a scenario with less or no symmetry, if helium detonations commence at multiple points, for example, the secondary detonation of the core is less certain. In their SPH simulations, García-Senz et al. (1999) first explored, using coarse resolution, the possibility of starting detonations at multiple points in the helium layer. In particular, they studied a case with asynchronous ignition at five points, finding that core detonation could still result from the collision of the various helium detonations.

If the core does not ignite, the helium explosion alone could produce a sub-luminous, “point Ia”, supernova (Bildsten et al. 2007). This raises the question as to how robust the triggering of the secondary core detonation is. If it is robust, a detonation of the helium shell alone might be very rare or even impossible.

We here revisit the double detonation scenario using some of the white dwarf models generated with KEPLER and presented in Woosley & Kasen (2011). Following a

description of the numerical methods in §2, we first discuss the results of simulations that test the viability of direct drive in §3.1. We then (§3.2) study sliding helium detonations that lead to a hot spot inside the core, with the helium detonation started at one, two or three points. The initiation of detonations in lightweight helium shells is investigated in §3.2.6. In §3.3, we present nucleosynthesis yields from runs following the complete detonation of white dwarfs. We end with a discussion and summary in §4.

## 2. NUMERICAL METHODS

### 2.1. Hydrodynamics

For our multi-dimensional studies we use the Eulerian hydrodynamics code CASTRO (Almgren et al. 2010; Zhang et al. 2011) to solve the equations for compressible fluid dynamics in combination with a nuclear reaction network. We employ an equation of state based on the Helmholtz free energy (Timmes & Arnett 1999; Timmes & Swesty 2000) and a 19 isotope network to compute energy generation and nucleosynthesis (the same as in KEPLER, see §2.2 for details). In many simulations, we make use of CASTRO’s capabilities for adaptive mesh refinement (AMR). The initial models for the multi-D CASTRO simulations presented here were constructed with the implicit Lagrangian hydrodynamics code KEPLER in 1D (Weaver & Woosley 1978; Woosley et al. 2002). The evolution of several helium-accreting white dwarfs was followed with a model for convection based on mixing-length theory, see Woosley & Kasen (2011). The CASTRO simulations start from KEPLER snapshots taken before a thermonuclear runaway sets in. Their key properties are listed in Table 1.

In Eulerian simulations, adding a relatively small amount of hot gas to a cold zone can raise the average temperature above the threshold for ignition, thus igniting the whole zone. Without any correction, the speed with which a “detonation front” propagates would thus be dependent on the size of the zones and driven entirely by artificial advection. To simulate detonation more realistically, we introduce a delay timer that suppresses the burning in a particular zone for half a sound crossing time. If, at any time, the necessary conditions for nuclear burning are not satisfied, the timer is set to zero. If they are satisfied, the timer starts counting and when half a sound crossing time (Courant time) has passed, nuclear burning processes are switched on in this particular zone.

In simulations of the whole star, the density of the artificial external medium is set to  $1 \text{ g cm}^{-3}$  and given the same temperature as the outer edge of the helium shell. This means that as the shock of the helium detonation breaks out of the star, it is accelerated by a very steep pressure gradient. As the time step of our simulations is limited by the largest fluid velocities or sound speeds in the entire domain, the calculations become very expensive. To contain the detrimental effect on the time step, we apply a velocity cap of  $1.5 \times 10^9 \text{ cm s}^{-1}$  in the ambient medium. To distinguish the ambient from stellar material at all times of the simulation, we give it a unique composition of 100%  $^{16}\text{O}$ . We used no velocity cap and lower ambient densities (starting with  $10^{-2} \text{ g cm}^{-3}$  and ending with  $10^{-5} \text{ g cm}^{-3}$  in the final computational box) in runs where the expansion of the ejecta was followed

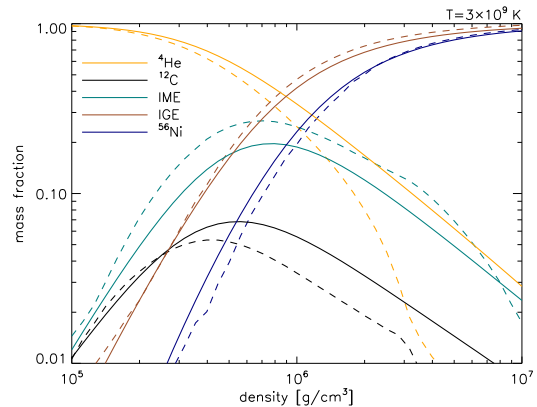


FIG. 1.— Variation of the final composition for a peak temperature of  $3 \times 10^9 \text{ K}$  when the density in the simulated explosion is varied from  $10^5$  to  $10^7 \text{ g cm}^{-3}$ . The solid and dashed lines represent the results obtained with the full network and the table, respectively.

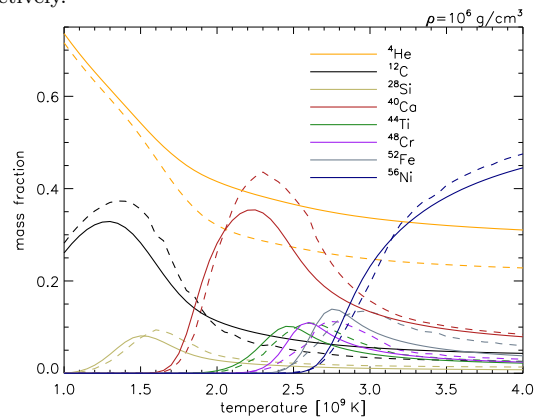


FIG. 2.— Variation of the final composition for a constant density of  $10^6 \text{ g cm}^{-3}$  when the peak temperature in the simulated explosion is varied from 1 to  $4 \times 10^9 \text{ K}$ . The solid and dashed lines represent the results obtained with the full network and the table, respectively.

(§3.3).

We generally make use of symmetries to reduce the computational load. With only one detonator, the problem is axisymmetric and its solution can be computed in 2D. For a simulation with two synchronous spherical detonators it is sufficient to do a 3D calculation of only a quarter of the star, with mirror symmetry at two boundaries (the  $x = 0$  and  $y = 0$  boundaries in our simulations). Two asynchronous detonators require a half-star simulation with mirror symmetry at one boundary (the  $x = 0$  boundary in our simulations).

### 2.2. Nuclear Energy Generation and Nucleosynthesis

Energy generation and approximate nucleosynthesis were calculated in all cases using a 19 isotope network with constituent species as defined by Weaver & Woosley (1978) and nuclear reaction rates updated to current values (Woosley & Heger 2007). Screening corrections were implemented for all rates. This network includes an “alpha-chain” ( $Z = N = 2n$ ,  $n$  = an integer) of nuclei from  $^{12}\text{C}$  through  $^{56}\text{Ni}$ , plus the species  $n$ ,  $p$ ,  $^3\text{He}$ ,  $^{14}\text{N}$ , and  $^{54}\text{Fe}$ . Simulated steady state links also approximate the presence of the odd  $Z$  isotopes from  $^{23}\text{Na}$  through  $^{55}\text{Co}$  (i.e., isotopes with  $Z = 2n + 1$ ,  $N = 2n + 2$ ). For this study, the photodisintegration of  $^{56}\text{Ni}$  to  $^{54}\text{Fe} + 2p$  was

TABLE 1  
WHITE DWARF MODELS

Model <sup>a</sup>	$M_{\text{core}}$ [ $M_{\odot}$ ]	$M_{\text{He}}$ [ $M_{\odot}$ ]	$r_{\text{core}}$ [km]	$\Delta r_{\text{He}}^b$ [km]	$r(T_{\text{max}})$ [km]	$T_{\text{max}}$ [ $10^8$ K]	$\rho(r(T_{\text{max}}))$ [ $10^6$ g cm $^{-3}$ ]	$\rho(r_{\text{core}})$ [ $10^6$ g cm $^{-3}$ ]	$\rho(r=0)$ [ $10^7$ g cm $^{-3}$ ]
A (8B)	0.801	0.143	4081	2080	4267	2.06	1.19	1.66	2.21
B (10B)	1.000	0.082	3616	1370	3765	2.42	1.30	1.93	5.67
C (10C)	1.000	0.091	3518	1380	3624	2.31	1.63	2.18	6.02
D (10HC)	1.002	0.045	4161	1260	4187	2.80	0.717	0.932	4.24
E (10HD)	1.001	0.078	3696	1350	3724	2.36	1.50	1.77	5.33

<sup>a</sup> The model identifiers in [Woosley & Kasen \(2011\)](#) are written in parentheses

<sup>b</sup> Approximate helium shell thickness, with the outer boundary defined where the density is 1/100 of the value at the core-shell interface

not allowed which meant that electron capture and  $^{54}\text{Fe}$  were essentially omitted from the network. Furthermore  $^1\text{H}$ ,  $^3\text{He}$ ,  $^{14}\text{N}$ ,  $n$ , and  $p$  never achieved any significant abundances, so the effective network really just contained the 13 alpha-chain isotopes. Past studies ([Timmes et al. 2000](#)) have shown that such a limited network gives good agreement with the results of much larger networks provided one is interested only in bulk nucleosynthesis and energy generation.

The network itself was employed in all carbon-rich zones always and, in most cases, for the helium shell. In some cases, however, it was computationally expedient to use a table that was prepared off-line using the network. Those cases included studies of helium shell detonation where the whole star was carried (§3.2), up until the generation of a hot spot in the core. The simulations for which detailed yields are given (§3.3) make use of the full network from beginning to end, as do the local simulations of direct drive (§3.1).

The use of a table here was novel and warrants some discussion. Unlike isobaric burning in e.g., carbon deflagration supernovae, the table here has to work reliably in dynamic situations where both the temperature and density are rapidly varying and where the outcome is sensitive to the time history of both. Using the network, a large table was generated using the results of many off-line studies of helium burning at constant temperature and density. Values of temperature in the range  $10^{8.5} - 10^{9.65}$  K ( $\Delta \log T = 0.05$ ) and density in the range  $10^5 - 10^{7.1}$  g cm $^{-3}$  ( $\Delta \log \rho = 0.10$ ) were included. Results of the burning – the composition, average binding energy per nucleon, and time derivative of the helium mass fraction, were sampled for 50 values of helium mass fraction ranging from 0.02 to 1.0 in steps of 0.02. To preserve accuracy, the rate equation for the helium mass fraction was divided by the leading order term in the  $3\alpha$  reaction rate, i.e.,

$$\left(\frac{dX_{\text{He}}}{dt}\right)_{\text{table}} = \left(\frac{dX_{\text{He}}}{dt}\right)_{\text{calc}} T_9^3 \left(\rho^2 X_{\alpha}^3 \exp\left(\frac{-4.403}{T_9}\right)\right)^{-1} \quad (1)$$

This resulted in a slowly varying function of  $T_9$ ,  $\rho$ , and  $X_{\alpha}$  in the table.

When using the table in a multi-dimensional simulation, triple variable interpolation in  $\log \rho$ ,  $\log T_9$ , and  $X_{\text{He}}$  gave the current composition and  $dX_{\text{He}}/dt$ . The current time step and  $dX_{\text{He}}/dt$  gave a new helium abundance at the end of the step. Another call to the table using the new helium abundance gave a revised composition for the other species, and the change in composition gives a

change in nuclear binding energy, hence an energy generation, and the process continued.

The shortcoming of this approach is that the entries in the table were generated at constant temperature. This neglects additional variables because a given temperature, density, and helium abundance can be reached by a variety of histories and the instantaneous abundances of the other nuclei are sensitive to which history was followed. Some additional rules are imposed to avoid unphysical and poorly behaved solutions. The helium abundance was only allowed to decrease, i.e.,  $dX_{\text{He}}/dt$  had to be negative, or no composition change or energy generation is allowed. Further, no modification of the composition occurred unless both the abundance of  $^{56}\text{Ni}$  and the nuclear binding energy increased during a time step. When these conditions were met, a change in composition was allowed, but the new composition was not just taken from the table. Instead a fraction of the new composition at the given temperature and density was added to the old one with that fraction determined by the change of the helium abundance during the step. Essentially this procedure partitions the nuclear evolution for an arbitrarily varying temperature and density history into a series of small steps taken at constant temperature and density. For the conditions of the problem, the requirement that the time step be a small fraction of the Courant time proved adequate to preserve accuracy.

To demonstrate the validity of the procedure, a series of simulated explosive helium burning studies were carried out off line using both the network and the table. Starting with a composition of pure helium, matter was expanded from a peak temperature,  $T_{90}$  at constant density on a time scale  $\tau$  such that

$$T_9(t) = T_{90} \exp(-t/\tau), \quad (2)$$

and the final composition examined when the temperature had declined below  $10^8$  K. The results are shown in Figs. 1 and Fig. 2. Figure 2 shows the variation of the final composition for a constant density of  $10^6$  g cm $^{-3}$  when the peak temperature in the simulated explosion is varied from 1 to  $4 \times 10^9$  K. In general the agreement between the network results and those obtained using the table is quite good. There is a substantial deviation of up to 50% in the final helium abundance for the higher temperature explosions. Using the table gives a smaller final abundance for helium because burning at a constant low temperature gives a smaller mean nuclear mass and charge than explosive burning cooling from a higher temperature to the same helium mass fraction, density and temperature. Lighter nuclei have larger cross sections for

TABLE 2  
DIRECT DRIVE: MASSES OF THE HELIUM DETONATION  
SPHERES AT CORE CONTACT

model	$r_{\text{detonator}}$ [km]	$\Delta r^a$ [km]	$M_{\text{He-sphere}}^b$ [ $10^6 \text{ g cm}^{-3}$ ]	works/fails
A	4270	189	$3.89 \times 10^{28}$	fails
A	4470	389	$2.80 \times 10^{29}$	fails
A	4670	589	$8.28 \times 10^{29}$	works
B	3765	149	$2.17 \times 10^{28}$	fails
B	3815	199	$4.75 \times 10^{28}$	fails
B	3865	249	$8.71 \times 10^{28}$	works
C	3624	106	$9.40 \times 10^{27}$	fails
C	3636	118	$1.26 \times 10^{28}$	fails
C	3649	131	$1.68 \times 10^{28}$	works
C	3674	156	$2.75 \times 10^{28}$	works
C	3724	206	$5.91 \times 10^{28}$	works

<sup>a</sup> Distance from the core-shell interface to the detonator center

<sup>b</sup> Defined as twice the mass of the helium contained in the half-sphere of radius  $\Delta r$  below  $z = r_{\text{detonator}}$

$\alpha$ -capture. One could improve the fit by adding a fourth independent variable, the mean nuclear charge (excluding helium itself), but the present approach was deemed adequate for this study. Some test runs at constant temperature and density using the table and the network gave near perfect agreement showing that the table had been correctly implemented.

Figure 1 shows the results for a series of explosions with constant peak temperature ( $3 \times 10^9 \text{ K}$ ) calculated for a variety of densities. For ease of plotting and because it most directly affects the energy generation, the species Si, S, Ar, and Ca have been combined into “intermediate mass elements” (IME) and the elements Ti, Cr, Fe, and Ni have been combined into “iron group elements” (IGE).  $^{56}\text{Ni}$  is also shown separately. The overall agreement between network and tables is again quite good.

### 3. RESULTS

#### 3.1. Direct Drive

Here we consider the possibility of a helium detonation wave that traverses the core-shell interface beneath its origin, directly igniting the core at the outer edge. Taking the  $(0.801 + 0.143)M_{\odot}$  white dwarf Model A as initial condition, we did a series of 2D simulations that cover a local region including the core-shell interface. The domain range in most cases is  $0 < R_8 < 1$  and  $3.3 < z_8 < 5.3$  in cylindrical coordinates  $(R, z)$ , the core-shell interface being at the spherical radius  $r_8 = 4.08$ . The grid resolution in most cases is  $0.977 \text{ km}$  (no AMR). The gravitational field is taken to be static and the boundary conditions are usually reflecting on all sides (as the detonation proceeds supersonically, the choice of boundary conditions is not critical). All simulations employed a full 19-isotope network which covers helium, carbon and oxygen burning. The detonation spots used to start the detonation had a radius of  $50 \text{ km}$ , a temperature of  $2 \times 10^9 \text{ K}$  at the center and  $1.8 \times 10^9 \text{ K}$  at the outer edge (linearly decreasing), a radial velocity of  $8000 \text{ km s}^{-1}$  at the outer edge (increasing linearly from zero) and twice the ambient density.

Figure 3 depicts snapshots of several cases. In the standard case (a), the helium detonator is centered at the radius at which the temperature is maximal,  $189 \text{ km}$  above

the core-shell interface. While the detonation creates an indentation in the interface, there is only little carbon burning and the detonation does not penetrate the core.

With the helium detonation initiated  $200 \text{ km}$  higher, case (b), the detonation penetrates into the core. The front is unstable though, developing dents filled with compressed material that fails to ignite. While it is possible that core ignition ensues from a detonation that fragments, we did not follow such pathological cases in our study and dismissed them as failures. In a similar simulation with half resolution ( $1.95 \text{ km}$ ), case (c), the front is stable. The oxygen starts to burn  $1130 \text{ km}$  below the interface (at  $72\%$  of the core radius), where the density exceeds  $5.3 \times 10^6 \text{ g cm}^{-3}$ .

With the helium detonation initiated  $400 \text{ km}$  above the temperature maximum, case (d), the detonation penetrates the core at our standard resolution, not showing any instabilities. We followed this detonation in a global simulation that encompasses half of the star, with the same resolution ( $\approx 1 \text{ km}$ ) as in the local simulation in a region that extends from the detonation spot to the center of the star ( $R_8 < 1$  and  $z_8 < 5$ ). This detonation stably proceeds all the way to the center. Oxygen burning starts  $830 \text{ km}$  below the interface (at  $80\%$  of the core radius).

The fronts of detonations started at different altitude have different curvatures when they hit upon the core-shell interface. This raises the question as to whether the curvature of the detonation front plays a key role. A detonator in the form of an oblate spheroid fares better than a spherical one, compare panels (e) and (a). However, the detonation front starts out considerably hotter than in the spherical case, which is possibly related to the details of how the detonation was started.

We also considered the possibility of a layer where helium mixes with core material. In case (f), we start with a mixture of  $70/20/10\%$   $^4\text{He}/^{12}\text{C}/^{16}\text{O}$  in the region  $3.98 < r_8 < 4.18$ , i.e.  $100 \text{ km}$  above and below the original core-shell interface. The detonation transcends into the core in this case. We surmise that a mixed layer on both sides of the interface effectively increases the distance from the detonator to the core, thus facilitating direct drive.

In cases (g) and (h), we start with a mixture of  $70/20/10\%$   $^4\text{He}/^{12}\text{C}/^{16}\text{O}$  and  $50/30/20\%$   $^4\text{He}/^{12}\text{C}/^{16}\text{O}$ , respectively, in a  $100 \text{ km}$  wide region above the original interface only. Although the detonation changes when it enters the mixed region, becoming hotter and faster, it fails to penetrate the core and stay intact in both cases. Even with half resolution, the detonation in case (g) shows the same instability (unlike case c, for which the coarser resolution helped to suppress instabilities in the detonation front). A mixture of  $80/20\%$   $^4\text{He}/^{12}\text{C}$  in a  $100 \text{ km}$  wide region also leads to failure (not shown in Fig. 3).

#### 3.1.1. Heavier Dwarfs

The above discussion shows that direct drive is not likely for Model A if the helium detonation starts where the gas is hottest, i.e., the most natural location for a detonator. Models B and C both have a denser  $1.0 M_{\odot}$  core which in principle should detonate more easily than the  $0.8 M_{\odot}$  core of Model A. Model C is slightly more



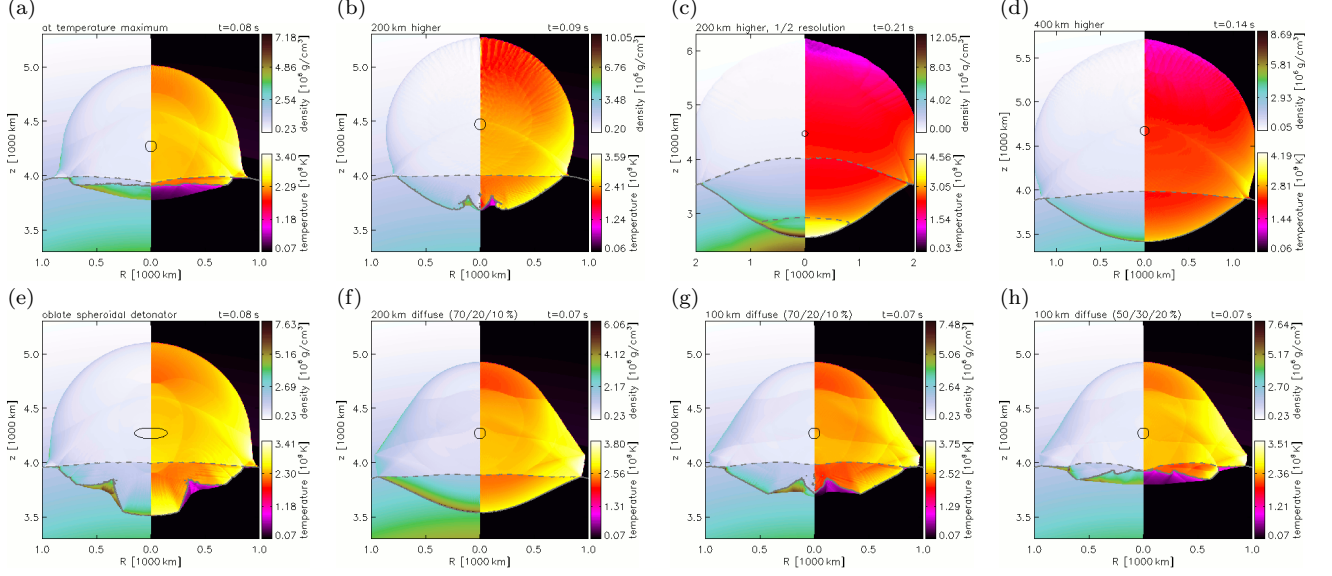


FIG. 3.— Density (left, upper colorbar) and temperature (right, lower colorbar) in local 2D simulations of helium detonations hitting upon the carbon-oxygen core. The black circles indicate the perimeters of the helium detonation spots at the beginning of each simulation. The solid and dashed gray lines represent the mass fraction contours for 49%  $^{12}\text{C}$  and 49%  $^{16}\text{O}$ , respectively.

compact than Model B.

Following a similar procedure, we tested for the possibility of direct ignition with detonators at different altitudes for these models. The radius of the detonation “hot spots” was 20 km and the distance between the core-shell interface and the temperature maximum was 149 km and 106 km in Models B and C, respectively. In both cases, direct ignition failed if the detonation was started at this altitude.

If we started the helium detonation 100 km above the hottest layer of Model B however, the detonation front smoothly transcended into the core. If ignited 50 km above the hot layer, the detonation fragmented and died upon passing into the core. In Model C, the direct drive worked with detonators at altitudes of 100 km, 50 km and even 25 km above the hottest layer. At 12 km, however, it failed<sup>1</sup>. These results for direct drive with detonators at different altitudes are summarized in Table 2.

To explore the relevant physics and test the accuracy of the CASTRO results, a series of calculations were carried out using the KEPLER code. These studies explored the critical mass for carbon detonation at the relevant densities. A hypothesis we wanted to explore was that the critical altitude for a successful propagation of the helium detonation into the carbon is given by the radius of the critical *carbon* mass required to generate a self-sustaining detonation at the density characterizing the carbon-helium interface. As we shall see, this hypothesis turned out to be approximately correct.

In the first study, spheres of 50% carbon, 50% oxygen were prepared with a constant density of  $1.93 \times 10^6 \text{ g cm}^{-3}$ , as appropriate to Model B. In a one-dimensional spherical region of variable radius, the tem-

perature was given a constant gradient (with respect to radius, not mass, even though the code is Lagrangian) with values ranging from  $2.8 \times 10^9 \text{ K}$  at the center to  $1.0 \times 10^8 \text{ K}$  at the edge. This 200 zone region was surrounded by 300 zones of carbon and oxygen at  $10^8 \text{ K}$ . All zones had the same radial thickness. The radius of the region with the temperature gradient was varied and its ability to generate a self-sustaining detonation determined. The central value of  $2.8 \times 10^9 \text{ K}$  is sufficiently high to guarantee carbon burning that was initially supersonic. This procedure is very similar to the one previously followed by Niemeyer & Woosley (1997), Röpke et al. (2007) and Seitenzahl et al. (2009).

For a “detonator” radius of 150 km, an initially strong detonation decayed away after traversing an additional 70 km of “cold” carbon and oxygen. For a radius of 200 km however, the detonation propagated successfully to the edge of the grid at 500 km. This is sufficiently far, considering that in the real star the density would have become higher and the detonation more robust. These detonators enclosed masses of  $2.73 \times 10^{28} \text{ g}$  (150 km) and  $6.47 \times 10^{28} \text{ g}$  (200 km) respectively.

More realistically, the detonator consists of helium, not carbon and oxygen and the background is better approximated as isobaric rather than constant density. A temperature of  $2.8 \times 10^9 \text{ K}$  in the carbon also implies an unrealistically high energy density not likely to be achieved at these low densities. A pure helium sphere with variable radius was surrounded by a thick shell of 50%  $^{12}\text{C}$  and 50%  $^{16}\text{O}$  again at  $1.93 \times 10^6 \text{ g cm}^{-3}$  with a temperature of  $1.0 \times 10^8 \text{ K}$ . The helium core was comprised of 200 Lagrangian mass shells of equal mass with a central temperature of only  $1.0 \times 10^9 \text{ K}$  and a temperature at the edge of  $1.0 \times 10^8 \text{ K}$  and a constant gradient (with respect to radius) in between. The large value of central temperature assured supersonic burning and the well zoned gradient implied the existence of a region in the helium where the phase speed of the burning was sonic. The density within the helium core was varied so as to provide a constant pressure equal to the pressure

<sup>1</sup> Given that this displacement is becoming comparable to the size of the detonator itself, it is questionable whether direct drive will or will not work for the most massive models. Also the exact location of the hot layer is probably not known to this precision due to the one-dimensional mixing length approximation used to treat convection. Multi-dimensional simulation of the convection during the pre-explosive runaway might provide additional insight.

in the carbon-oxygen layer. Thus pressure on the entire grid was initially  $7.25 \times 10^{22} \text{ dyne cm}^{-2}$ . Gravity was neglected and the pressure was initially held constant by applying a boundary pressure equal to the pressure on the grid. If the radius of the helium sphere was 211 km enclosing  $6.37 \times 10^{28} \text{ g}$ , the detonation successfully propagated into the surrounding carbon. Another run with a helium sphere radius of 159 km ( $2.69 \times 10^{28} \text{ g}$ ) failed to detonate the carbon shell however.

These results are in good qualitative agreement with those obtained using a 2D representation of the full star in the CASTRO code (Table 2). They also agree reasonably well with the pure carbon-oxygen study at constant density described above. Apparently the critical altitude (or detonator radius) is not very sensitive to the different energy yields of carbon and helium burning. This is somewhat surprising, but confirms the hypothesis that the critical altitude in the helium layer is one that would enclose the critical mass of carbon required for detonation at the interface density.

### 3.2. Shock Collisions and Hot Spots

To study the sliding helium detonation and the internal compressional wave which potentially produces the seed for a core detonation, we suppress nuclear burning in zones with more than 10%  $^{12}\text{C}$ . This is to prevent spurious carbon burning at the core-shell boundary due to the mixing of hot helium with cold carbon in a zone, and to prevent core detonation before the waves in the core have fully converged and produced the highest possible temperatures and densities (which we want to determine). For the sake of comparability, we here focus on the  $(0.801 + 0.143)M_{\odot}$  Model A for the most part. The detonation of dwarfs with  $1.00M_{\odot}$  cores and lightweight helium shells is discussed in §3.2.6.

#### 3.2.1. One Detonator

We here consider the case of a single, spherical detonation spot setting off a helium detonation where the hottest layer (at  $r_8 = 4.27$ ) intersects with the positive  $z$ -axis in our coordinate system. Runs 1, 4, 5 and 11 all represent this case with different numerical resolutions. The helium detonation wave wraps around the star (see Fig. 4a) and reaches the antipode of the detonator after about 1.2s. For comparison, a sound wave in the helium shell would need about 5.6s to reach the other side of the star. This corresponds to a front velocity of  $\sim 1.1 \times 10^9 \text{ cm s}^{-1}$ . The polar (latitudinal) velocity of the ash directly behind the front and the sound speed in the ash both are roughly  $6.9 \times 10^8 \text{ cm s}^{-1}$ . Their sum is larger than the actual front velocity, consistent with incomplete burning rather than a Chapman-Jouguet detonation (cf. Sim et al. 2012). The  $^{56}\text{Ni}$  fraction far ( $\sim 1000 \text{ km}$ ) behind the detonation front is about 70%.

The sliding detonation induces an internal compressional wave which converges off-center inside the core on the  $z$ -axis (in general: the axis of symmetry in the problem). The average velocity with which the perturbation propagates in negative  $z$ -direction from the helium ignition point to the final convergence point is  $\sim 4.0 \times 10^8 \text{ cm s}^{-1}$ , a little larger than the mean sound speed inside the core ( $3.4 \times 10^8 \text{ cm s}^{-1}$ ).

The temperatures and densities in some zones of run 1

are high enough to potentially<sup>2</sup> trigger a core detonation where the internal wave finally converges (Niemeyer & Woosley 1997; Röpke et al. 2007; Seitenzahl et al. 2009). However, it is likely that the core ignites earlier, at larger distance from the center and close to the core-shell interface on the  $z$ -axis, where the internal wave front converges in the polar direction (but not in radial direction), and the converging helium detonation drives a hot, thin inflow of  $^{56}\text{Ni}$  in positive  $z$ -direction. As a numerical experiment, we restarted run 1 without suppressing the burning of carbon-rich zones at times  $t = 1.2 \text{ s}$  (when the helium detonation converges),  $1.3 \text{ s}$ ,  $1.4 \text{ s}$ , and  $1.5 \text{ s}$  (when the internal wave converges). In all of these cases, a detonation wave in the core forms immediately.

The values of the density and temperature in the hot spot are dependent on the spatial resolution  $\Delta x$  of the grid as well as on the temporal separation  $\Delta t$  of the considered snapshots (for practical reasons, we do not edit and analyze the results at every time step), cf. the values of temperature and density in the hot spots of runs 1, 4, 5 and 11 listed in Table 3. However, all results unequivocally indicate that the core would detonate. We expect that a higher resolution would only increase the likelihood for detonation.

#### 3.2.2. Opposite Detonators

As a limiting case of multi-point ignition, we at first consider two detonators at opposite points in the helium shell (run 2). While it is unlikely for such detonators to be synchronous, this poses a computationally cheap 2D problem which can be regarded as a numerical experiment. The internal waves in this case collide on the  $z = 0$  plane (the detonators being centered on the  $z$ -axis at  $z_8 = \pm 4.27$ ), beginning at the outer edge of the core at  $t = 0.60 \text{ s}$  and reaching the center at  $t = 1.05 \text{ s}$ . The final wave collision in the central part of the star takes place on a  $\sim 1400 \text{ km}$  wide disk without generating a discernible hot spot. However, temperatures  $\gtrsim 10^9 \text{ K}$  occur on the collision plane at large radii ( $r_8 \sim 1.8 \dots 3.2$ ). While the material is not compressed there, we observe a radially inward moving core detonation in a run where the burning of carbon is allowed for  $t \geq 0.65 \text{ s}$ . If carbon burning is suppressed, the original core waves are reflected at the  $z = 0$  plane. The reflected waves collide on the  $z$ -axis (symmetrically on both sides of the  $z = 0$  plane), creating dense hot spots at  $z_8 = \pm 1.45$  that would very likely have ignited the core if ignition had failed earlier.

When one of the detonators (in our case the one on the negative side of the  $z$ -axis) is delayed by  $0.30 \text{ s}$ , the two helium detonation fronts collide at  $t = 0.75 \text{ s}$  at an angle of  $112^\circ$  with respect to the positive  $z$ -axis, see Fig. 5. As in the synchronous case, the collision of the primary internal waves, which here happens on a slightly curved disk at  $z \approx -600 \text{ km}$ , does not generate a hot spot. However, a wave reflected toward the negative  $z$ -axis produces a hot spot that is sufficiently dense to trigger core

<sup>2</sup> Whether a spontaneous detonation initiates depends not only on the density, the peak temperature and the size of the region (or, equivalently, its mass), but also on the shape of the temperature profile (as emphasized by Seitenzahl et al. 2009). The conditions in the hottest zone are listed in Table 3. Since the grid zones in our simulations are usually larger than the critical masses for detonation, it is not possible to predict with certainty whether the conditions in one or a few zones lead to detonation.

TABLE 3  
CONDITIONS AT THE HOT SPOT INDUCED BY CONVERGING COMPRESSIONAL WAVES IN THE CORE

Run	Model	$\alpha^a$	$\tau^b$ [s]	$\Delta x^c$ [km]	$\Delta t^d$ [s]	$t$ [s]	$z$ [ $10^8$ cm]	$r^e$ [ $10^8$ cm]	$T$ [ $10^9$ K]	$\rho$ [ $10^7$ g cm $^{-3}$ ]	Type $^f$
1	A	—	—	6.51	0.05	1.50	−1.90	1.90	5.25	6.21	p
2	A	180°	—	6.51	0.05	1.40	$\pm 1.45$	1.45	1.93	3.55	r
3	A	180°	0.30	6.51	0.05	1.45	−1.72	1.72	3.34	4.00	r
4	A	—	—	14.6	0.02	1.48	−1.87	1.87	8.09	2.68	p
				3.66 $^g$	0.02	1.48	−1.92	1.92	9.61	2.54	p
5	A	—	—	25.0	0.05	1.55	−1.96	1.96	3.09	4.29	p
				25.0	0.005	1.515	−1.91	1.91	5.51	20.9	p
6	A	54°	—	25.0	0.05	1.40	−1.76	1.77	2.81	5.66	p
7	A	54°	0.15	25.0	0.05	1.45	−1.74	1.80	3.67	9.51	p
8	A	90°	—	25.0	0.05	1.40	−1.39	1.54	2.17	5.04	t
9	A	120°	0.30	25.0	0.05	1.50	−0.91	1.96	2.86	3.59	t
10	A	120°, 90°, 100°	0.30, 0.20	25.0	0.05	1.45	−0.71	1.65	2.19	5.27	t
11 $^h$	A	—	—	52.1	0.05	1.55	−1.95	1.95	2.96	7.56	p
12	A	36°	—	52.1	0.05	1.45	−1.74	1.74	2.19	4.93	p
13	A	54°	—	52.1	0.05	1.45	−1.74	1.81	2.00	4.24	p
14	E	—	—	6.51	0.05	1.40	−1.70	1.40	3.52	4.54	p
15	E	180°	—	6.51	0.05	0.60	0	3.48	3.48	0.60	b
16	D	—	—	6.51	0.05	1.80	−2.13	2.13	2.44	3.31	p
17	D	180°	—	6.51	0.05	—	—	—	—	—	—

<sup>a</sup> Angular separation(s) of the detonators in cases with multiple detonators

<sup>b</sup> Delay of the second (and third) detonator

<sup>c</sup> Grid resolution at the highest AMR level that includes the hot spot

<sup>d</sup> Cadence of the considered snapshots

<sup>e</sup> Distance from the center (spherical radius)

<sup>f</sup> Type of listed hot spot: (p) where primary waves converge, (r) where reflected waves collide, (t) where a wave passes through others and converges or (b) near the core boundary, where primary waves first collide

<sup>g</sup> Restarted with finer zoning in the region where the internal wave converges

<sup>h</sup> Despite this being a 2D problem, this run was done in 3D

detonation.

### 3.2.3. Two Synchronous Detonators

Before discussing 3D cases of two-point ignition in the helium, it is worth noting that a single, small aspherical detonator is virtually equivalent to a spherical one, regardless of how strongly deformed it is (as long as it sets off a detonation). As the detonation expands with constant velocity in every direction, the original asphericity is quickly lost. To assess the effects of non-axisymmetry on the focusing of the internal waves, we therefore consider cases with two detonators at varying but significant separation from one another.

In cases with two moderately separated, synchronous detonators (we consider angular separations of 36°, 54° and 90°), the initially separate helium detonation fronts collide halfway between the two spots on the geodesic connecting them on the core surface, in our case the positive  $z$ -axis. While the detonations merge, the combined front proceeds toward the antipode of this collision point. The front initially has a head start on the plane that connects the two spots with the center of the star (the  $x = 0$  plane in our simulations), but the deficit becomes smaller as the detonations continue to merge<sup>3</sup>. As it approaches the antipode, the detonation front has the shape of a pointed ellipse. This shape can easily be understood considering the combined detonation as a su-

perposition of two detonations: the pointed ellipse is the intersection between two circles (or, more precisely, lines of constant latitude, if the ignition points are regarded as poles) whose centers are the respective antipodes of the ignition points. In a simulation, the detonation finally converges when the width of the pointed ellipse approaches the size of a grid zone. Theoretically, the ratio of the length of the ellipse compared to its width increases indefinitely, i.e., the wave always converges in a line rather than a point and the difference between having one and two detonators should become larger with increasing grid resolution or diffusion length.

In cases with 36° and 54° detonator separation, the region in which the internal waves converge becomes sufficiently hot and dense to trigger a core detonation, see Table 3 and Fig. 4b. We explicitly confirmed this for run 13 by switching on carbon burning for  $t > 1.40$  s. When two synchronous detonators are 90° apart (run 8), there is no hot spot at the site where the two primary waves converge at the  $z$ -axis (in general: the intersection of the two planes of symmetry in this problem). However, the waves induced by the two detonators pass through one another and form two hot spots at considerable distance (660 km) from the  $z$ -axis, see Fig. 4c.

### 3.2.4. Two Asynchronous Detonators

We next consider a case of two asynchronous detonators with an angular separation of 54°, run 7. Note that this scenario is less symmetric than the case of two synchronous detonators, there being only one mirror symmetry in the problem, across the plane which intersects both detonators. One of the detonators—the one on the  $+y$  side in our simulations—is set off 0.15 s (roughly half the time needed for the first detonation to reach the sec-

<sup>3</sup> For comparison, consider two merging detonations in a plane, starting from the  $x$ -axis at  $\pm a$ . With  $r$  being the radius of an individual detonation, the height of the combined detonation on the  $y$ -axis is  $\sqrt{r^2 - a^2}$ , asymptotically approaching  $r$  (and not  $r - a$ ) at large radii. That is, the two initially separate detonations become indistinguishable when their size is much larger than the initial separation.



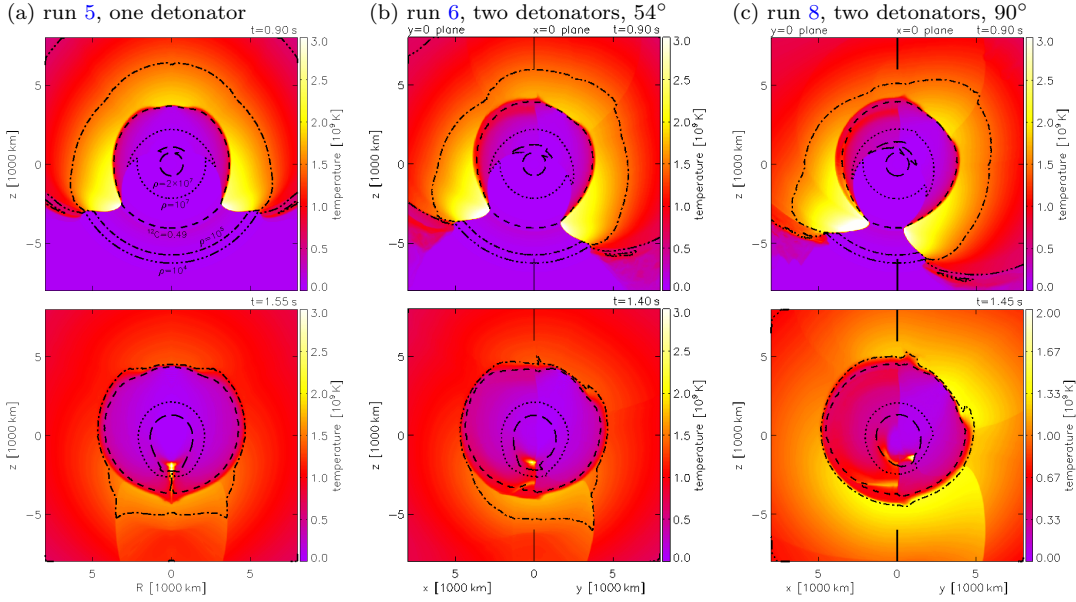


FIG. 4.— Snapshots of simulations with one (a) and two synchronous detonators (b:  $54^\circ$  separation, c:  $90^\circ$  separation) during the helium detonation stage (upper panels) and during the presence of a hot spot in the core (lower panels). Panels (b) and (c): the  $x = 0$  plane (right half), which contains the two detonators and the center of the star, is symmetric with respect to the  $y = 0$  plane (left half) and vice versa; the long ticks at  $R = 0$  indicate that these plots show not one but two orthogonal planes. The black contour lines represent, from the center outwards:  $\rho = 2 \times 10^7 \text{ g cm}^{-3}$  (long dashed),  $\rho = 10^7 \text{ g cm}^{-3}$  (dotted),  $X_C = 0.49$  (dashed),  $\rho = 10^5 \text{ g cm}^{-3}$  (dot-dashed) and  $\rho = 10^4 \text{ g cm}^{-3}$  (dot-dot-dot-dashed).

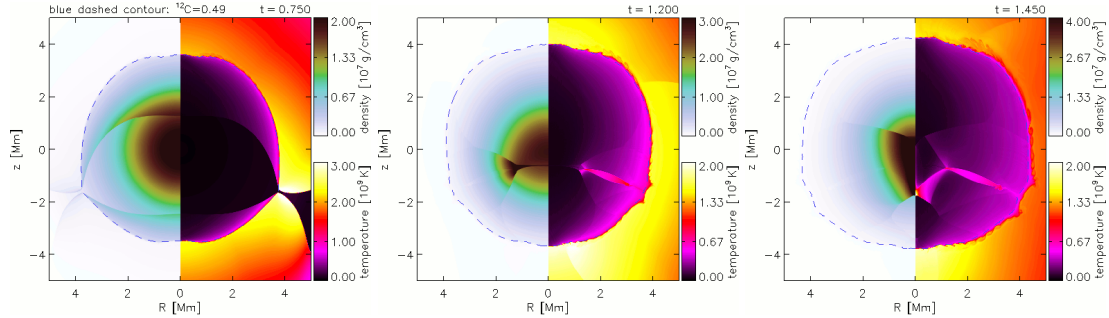


FIG. 5.— Three snapshots of a 2D simulation with asynchronous detonators on opposite sides (run 3): when the helium detonation fronts collide (left), when the internal wave converges (middle) and when reflected waves produce a hot spot (right). The blue dashed line indicates the core-shell boundary. Only the inner part of the simulation box is shown.

ond detonator) after the first one<sup>4</sup>. Shortly before converging, the helium detonation front assumes the shape defined by the intersection of two circles with different radii, see Fig. 6. The same shape can be seen in the internal wave front on concentric spherical surfaces. Just like in the synchronous case (run 6), a dense hot spot forms when the internal wave fronts converge, see Fig. 7 and the rightmost snapshot in Fig. 6.

With  $120^\circ$  separation and a delay of 0.30 s, run 9, there is no hot spot where the internal waves from the two detonators converge. As in the case with synchronous detonators at  $90^\circ$  discussed above, the waves from the two detonators pass through one another. The wave from the first detonator is the first to converge and trigger a core detonation.

### 3.2.5. Three Asynchronous Detonators

Unlike the above cases, a setup with three or more detonators is in general free of symmetries and requires

<sup>4</sup> We implemented this in the code by suppressing the time-step update of the zones comprising the detonation spot for said time.

a 3D simulation of the full star. In run 10, we again consider two detonators (A,B) with a separation of  $120^\circ$ , one of which (B) is delayed by 0.30 s, exactly as in run 9. In addition, a third detonator C, delayed by 0.20 s, is placed  $90^\circ$  from detonator A and  $100^\circ$  from detonator B on the positive  $x$  side. In this case, when the helium detonation converges toward the last patch of unburnt helium, it roughly has a triangular shape. The same shape is present in the internal wave on concentric spherical surfaces. There is a distinct hot spot when the internal waves converge. Shortly after, a secondary hot spot arises as the wave induced by the first detonator converges again with itself. Fig. 8 shows snapshots of both hot spots (right hand panels) and the converging wave fronts from which they originate (left hand panels).

### 3.2.6. Light Helium Shells

A detonation in a  $0.078M_\odot$  helium shell on top of a solar mass core (Model E, run 14) is set off by a 25 km spherical detonator centered on the hottest helium layer. The sliding helium detonation yields a distinct hot spot



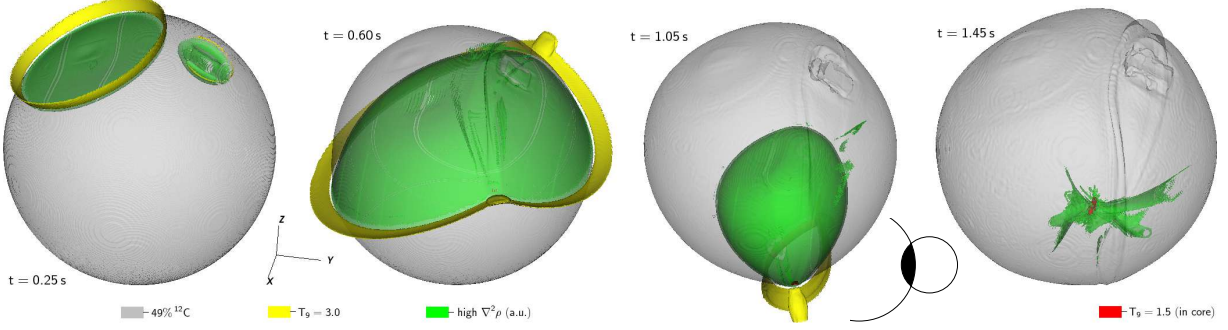


FIG. 6.— Helium shell detonation started by two asynchronous detonators with a  $54^\circ$  separation in the hottest helium layer (run 7). The gray, yellow and green isosurfaces indicate the boundary of the CO core, the detonation front and the internal compressional wave, respectively. The sketch next to the snapshot at  $t = 1.05$  s (second from right) qualitatively mimics the shape of the converging detonation front as the intersection of two circles. Red isosurfaces indicate the hot spot that is generated when the internal wave converges (rightmost snapshot).

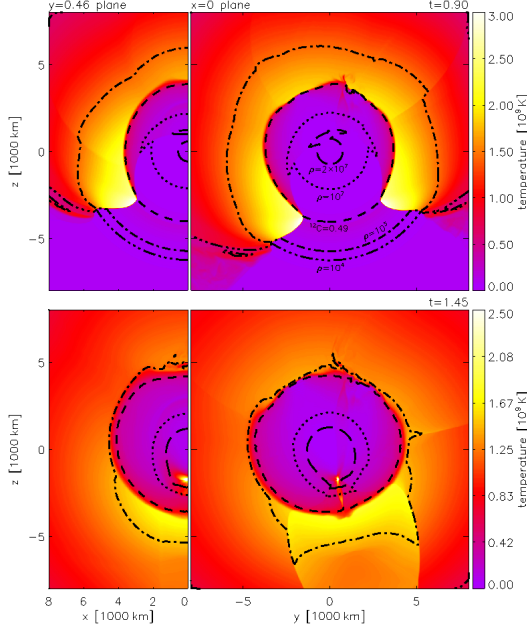


FIG. 7.— Snapshots of the temperature in a simulation with two asynchronous detonators at  $\pm 27^\circ$  from the positive  $z$ -axis on the  $x = 0$  plane (run 7). The  $x = 0$  plane (right panels) contains the detonators and the center of the star, and the orthogonal  $y_8 = 0.46$  plane (left panels) contains a hot spot generated by converging internal waves. The detonator on the positive side of the  $y$ -axis is delayed by 0.15 s. The black contour lines represent, from the center outwards:  $\rho = 2 \times 10^7 \text{ g cm}^{-3}$  (long dashed),  $\rho = 10^7 \text{ g cm}^{-3}$  (dotted),  $X_C = 0.49$  (dashed),  $\rho = 10^5 \text{ g cm}^{-3}$  (dot-dashed) and  $\rho = 10^4 \text{ g cm}^{-3}$  (dot-dot-dot-dashed). The snapshot at the bottom is taken when the internal wave fronts converge.

where the internal wave converges at  $t \approx 1.40$  s. With carbon burning turned on from the time when the helium detonation converges ( $t \approx 1.10$  s), the core immediately detonates near its surface. This detonation is triggered by a thin, hot radial inflow of  $^{56}\text{Ni}$ . As shown in the upper panel of Fig. 9, temperatures of  $2\text{--}4 \times 10^9$  K and densities on the order of  $10^7 \text{ g cm}^{-3}$  are generated along this jet. In a simulation with two synchronous, opposite detonators, run 15, temperatures  $> 10^9$  K are generated neither when the wave fronts converge at the center, nor along the  $z$ -axis when the reflected waves collide (in contrast with Model A, run 2). The only region hot enough to light the core in this case is located at the equatorial plane near the core's surface, where the collision of the internal waves begins. Although there is no hot inflow

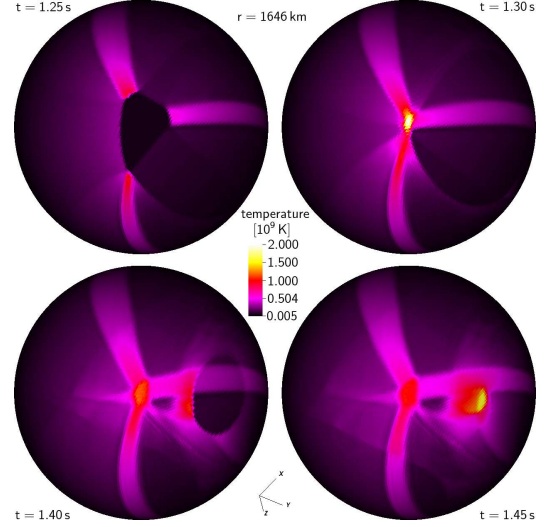


FIG. 8.— Snapshots of the temperature in a simulation with three detonators (run 10) on a concentric sphere inside the core which contains the hot spot from the three converging waves (upper right panel) as well as the hot spot from the wave induced by the first detonator alone (lower right panel).

TABLE 4  
DETONATIONS STARTED IN A SPHERICAL CAP

altitude <sup>a</sup> [km]	arc length [km]	rim density	rim velocity [ $10^8 \text{ cm s}^{-1}$ ]	detonates
0	141	$2 \times \text{ambient}$	8	yes
0	96	$2 \times \text{ambient}$	8	no
0	233	ambient	8	yes
0	141	ambient	8	yes <sup>b</sup>
0	96	ambient	8	no
0	415	ambient	1	yes
0	233	ambient	1	no
0	415	ambient	0.5	no
0	781	ambient	0.5	yes <sup>b</sup>
25	785	ambient	1	yes
25	418	ambient	1	no

<sup>a</sup> Radial distance from the hottest helium layer to the center of the cap

<sup>b</sup> Detonation moves only inward at first and is then reflected back

comparable to the case with one detonator (note that a radial inflow in this case is not a jet), see lower panel in Fig 9, the core there ignites in the simulation.

It is difficult to set off a detonation in a  $0.045 M_\odot$  helium shell surrounding a one solar mass core (Model D).

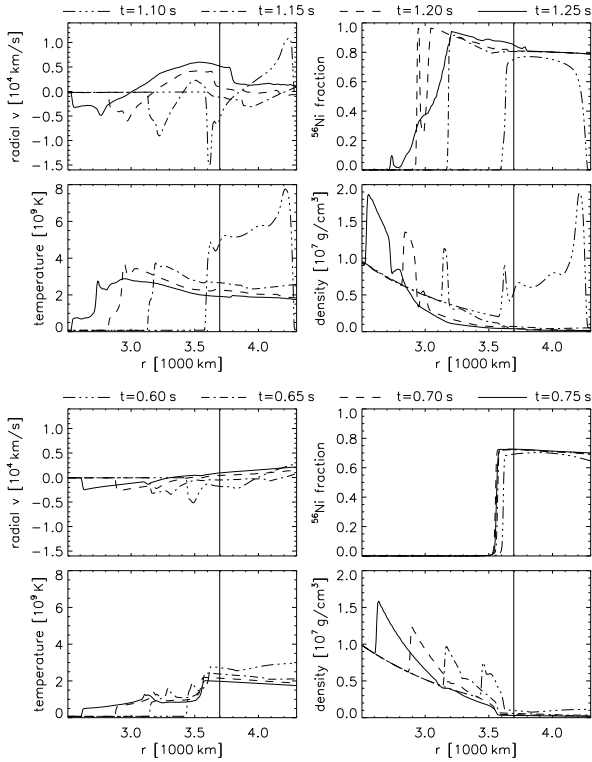


FIG. 9.— Conditions near the core boundary as a function of distance from the center. Top panel: on the line (negative  $z$ -axis) where the helium detonation front converges in a run with one detonator (run 14). Bottom panel: on the helium collision plane ( $z = 0$ ) in a run with two opposite synchronous detonators (run 15). The vertical lines mark the initial radius of the core-shell interface. The plots represent calculations where carbon burning is suppressed; otherwise the core ignites at the earliest time (dot-dot-dot-dashed line) in both cases.

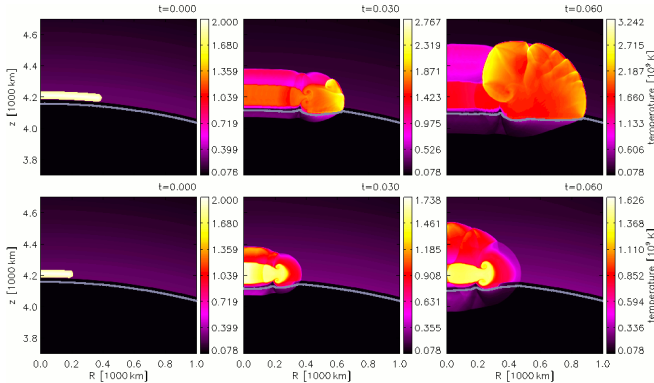


FIG. 10.— Successful (top) and unsuccessful (bottom) initiation of a detonation in the helium shell of Model D with a detonator in the form of a spherical cap. The cases shown are the last two in Table 4. The color bar ranges from the minimum to the maximum temperature in each plot (note the decline of the maximum in case of failure). The gray contour line, at 49%  $^{12}\text{C}$ , marks the core-shell interface.

We did not succeed with a spherical detonator centered on the hottest helium layer, whose density is  $7.17 \times 10^5 \text{ g cm}^{-3}$ . A detonation does not start even with a (perhaps unrealistically) strong initial detonator: a central temperature of  $3 \times 10^9 \text{ K}$ , linearly decreasing to  $1.5 \times 10^9 \text{ K}$  at the outer edge, a density three times that of the ambient medium and a radius of 25 km (ending 1 km above the core-shell interface). Large shock

velocities (we tried  $1.6 \times 10^9 \text{ cm s}^{-1}$  instead of our usual  $8 \times 10^8 \text{ cm s}^{-1}$ ) at the outer edge of the detonation spot did not help either.

A detonation in the  $0.045 M_{\odot}$  shell of Model D can be set off, however, by a large spherical detonator of radius 50 km (which is about twice the distance between the core-shell interface and the hottest helium layer) centered 25 km above the hottest helium layer. The resulting detonation front is more feeble than in all cases with heavier helium shells, blowing out at too coarse a resolution ( $\lesssim 2 \text{ km}$  works,  $6.5 \text{ km}$  does not), but once started, the detonation can propagate around the star.

We consider the possibility of a thermonuclear runaway starting in a (curved) sheet on an equipotential, instead of a single point. The size of convective cells in the helium shell is expected to be on the order of the pressure scale height, which is 366 km at the hottest helium layer in Model D. The size of the region where the runaway starts could be a substantial fraction of this, but is probably not larger. As a toy model, we consider detonation spots in the form of spherical caps with a thickness of 50 km. Selected runs are listed in Table 4 and examples for a successful and an unsuccessful detonation are shown in Fig. 10. As in most of our detonators, the temperature decreases linearly from  $2 \times 10^9 \text{ K}$  at the center to  $1.8 \times 10^9 \text{ K}$  at the outer edge (on all sides of the cap). The outer rims of the caps are half tori, imposed with a velocity that increases linearly from the torus center to the outer edge. An arc length of 50 km constitutes a limiting case in which the cap degenerates into a sphere with the same properties as our spherical detonators. The cap detonator is more powerful than a spherical one. Detonations can be initiated at ambient density with subsonic starter velocities. Smaller sizes require harsher starting conditions. Below a size of  $\sim 100 \text{ km}$  (roughly  $1/3$  pressure scale height), the initiation of a detonation appears impossible.

A helium detonation started by a single detonator<sup>5</sup>, run 16, converges after  $\approx 1.40 \text{ s}$ . The corresponding front velocity is  $\sim 9.4 \times 10^8 \text{ cm s}^{-1} \approx 4.3$  times the sound speed in the hottest helium layer. When the internal wave induced by the helium detonation converges 0.40 s later, it forms a distinct hot spot. Without suppression of the carbon burning, the core detonates immediately after the convergence of the helium detonation, starting at the  $z$ -axis near the core-shell boundary. In a simulation with two synchronous, opposite detonators, run 17, no hot spot is formed in the core. With carbon burning turned on, the core does not detonate in the simulation.

### 3.3. Complete Detonations

Table 5 lists the yields from helium shell detonations in different models, measured at the time when the helium detonation converges opposite the detonator (we only consider single detonators here, not expecting the yields from detonations started at multiple points to be much different). The lightweight helium shell of Model D yields little  $^{56}\text{Ni}$  but relatively large amounts of intermediate mass elements (e.g.,  $^{44}\text{Ti}$  and  $^{48}\text{Cr}$ ).

<sup>5</sup> We note that in order to sustain the helium detonation, the shell needs to be more finely resolved than in the other models. We here used 1.53 km. A resolution of 6.51 km is insufficient, causing the helium detonation to blow out quickly.

TABLE 5  
NUCLEOSYNTHESIS YIELDS IN THE HELIUM SHELL [ $M_{\odot}$ ]

	Model A	Model E	Model D
$^{12}\text{C}$	$8.00 \times 10^{-4}$	$5.24 \times 10^{-4}$	$7.02 \times 10^{-4}$
$^{14}\text{N}$	$1.11 \times 10^{-10}$	$2.83 \times 10^{-14}$	$4.24 \times 10^{-13}$
$^{16}\text{O}$	$3.19 \times 10^{-4}$	$1.93 \times 10^{-4}$	$2.46 \times 10^{-5}$
$^{20}\text{Ne}$	$4.78 \times 10^{-5}$	$2.72 \times 10^{-5}$	$1.95 \times 10^{-5}$
$^{24}\text{Mg}$	$9.40 \times 10^{-5}$	$5.30 \times 10^{-5}$	$3.00 \times 10^{-5}$
$^{28}\text{Si}$	$4.46 \times 10^{-4}$	$2.65 \times 10^{-4}$	$2.03 \times 10^{-4}$
$^{32}\text{S}$	$2.88 \times 10^{-4}$	$1.26 \times 10^{-3}$	$2.17 \times 10^{-4}$
$^{36}\text{Ar}$	$4.55 \times 10^{-4}$	$2.65 \times 10^{-4}$	$4.62 \times 10^{-3}$
$^{40}\text{Ca}$	$2.15 \times 10^{-3}$	$1.26 \times 10^{-3}$	$2.17 \times 10^{-3}$
$^{44}\text{Ti}$	$4.14 \times 10^{-3}$	$2.33 \times 10^{-3}$	$4.29 \times 10^{-3}$
$^{48}\text{Cr}$	$4.24 \times 10^{-3}$	$2.36 \times 10^{-3}$	$4.39 \times 10^{-3}$
$^{52}\text{Fe}$	$7.81 \times 10^{-3}$	$4.34 \times 10^{-3}$	$5.69 \times 10^{-3}$
$^{54}\text{Fe}$	$1.80 \times 10^{-5}$	$2.57 \times 10^{-6}$	$5.16 \times 10^{-7}$
$^{56}\text{Ni}$	$7.05 \times 10^{-2}$	$3.71 \times 10^{-2}$	$1.95 \times 10^{-3}$

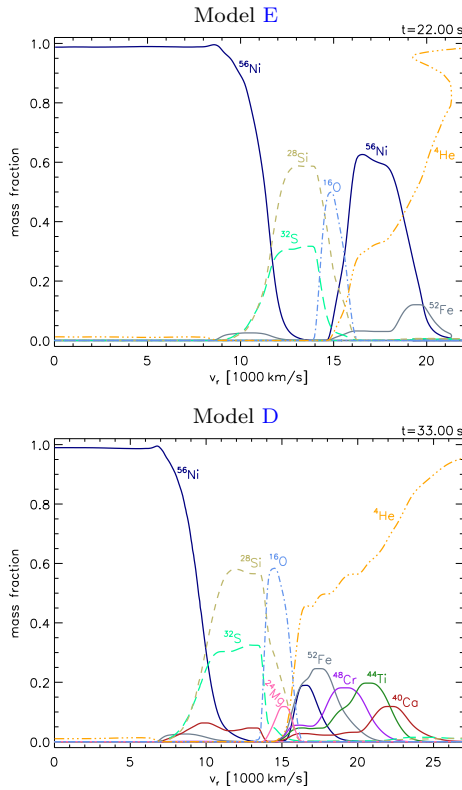


FIG. 11.— Mass fractions of elements along the equatorial plane ( $z = 0$ ) in the ejecta of Models E (top panel) and D (bottom panel) after complete shell and core detonations, as functions of radial velocity (which is approximately proportional to radius). In both panels, only elements with maximum fractions  $> 10\%$  are plotted, respectively.

We followed the detonation of the core and the expansion of the ejecta to scales of  $10^6$  km (about 200 times the size of the initial dwarf), at which time the expansion is homologous. The total nickel yields in Models A, D and E is  $0.38M_{\odot}$ ,  $0.52M_{\odot}$  and  $0.66M_{\odot}$ , respectively. Mass fractions of selected elements in Models E and D are plotted in Fig. 11. The inner parts of the core turn into almost pure  $^{56}\text{Ni}$  in both cases, whereas the outer parts yield mainly  $^{28}\text{Si}$  and  $^{32}\text{S}$ . The lighter helium shell produces large fractions of several intermediate mass elements instead of  $^{56}\text{Ni}$ , which is the dominant product

of the heavier shell.

#### 4. SUMMARY AND DISCUSSION

We studied the double detonation scenario for Type Ia supernovae by means of 2D and 3D simulations. Starting from the results of 1D stellar evolution simulations, we find that the helium detonation wave is halted at the core-shell interface if the detonation starts in the hottest layer, which in general is located at some altitude above the interface. If the detonation commences at higher altitude, the detonation may transcend into the core. For direct drive to be successful, the helium detonation must involve a critical mass which is sensitive to the density at the core-shell interface. A layer of mixed core-shell material does not facilitate the direct drive.

We confirm that the sliding helium detonation induces a mildly supersonic compressional wave inside the core which, if the detonation is set off at a single point in the helium shell, converges to produce an off-center spot that is sufficiently hot and dense to light the core as well. We tested the robustness of this model for non-symmetric initial conditions, considering a series of scenarios in which the helium detonation is started at two points and one scenario in which it is started at three points. We find that the secondary core detonation is quite robust, despite the lack of symmetry. In cases where detonators are widely separated ( $\gtrsim 90^\circ$ ), the hot spot is produced by reflected waves or waves that have passed through other waves before converging with themselves, rather than the converging primary waves. Only in one extreme case—two antipolar, synchronous detonators in the helium shell of a  $(1.002 \pm 0.045)M_{\odot}$  dwarf—we find no hot spot and no core ignition.

The generation of a detonation-inducing hot spot is robust even in a completely non-symmetric setup with three asynchronous detonators. Geometric arguments suggest that it is even more robust than a setup with two detonators, where the helium detonation and the core waves converge in an elongated region. As the elongation increases with the smallest possible separation of the detonation fronts, the difference of having one, two or three detonators might be larger at higher resolution. Although we have not run cases with more than three detonators, we expect that the core ignition would not be thwarted by additional detonators. A case with numerous detonators may be similar to a detonation in a spherical shell.

After the helium detonation has converged, the internal waves converge in polar (latitudinal) direction at ever decreasing radii, beginning right beneath the core-shell interface. In addition, the collision of the helium detonation front can drive a jet of hot ash into the core. In any case, this region has high ignition potential. That is, the core may ignite at large radii before the “proper” hot spot forms deeper inside as the wave fronts converge also in the radial direction. The complete convergence of internal waves may only happen in cores that are difficult to ignite.

Our simulations suggest that it is very hard, perhaps impossible under realistic assumptions, to initiate a helium detonation at densities  $\lesssim 10^6 \text{ g cm}^{-3}$  (as observed in plane-parallel geometry by Townsley et al. 2012). On the other hand, the yields from white dwarfs with thin helium shells are most compatible with observed Type Ia

supernovae. Detonations in the helium are more easily started in an extended sheet rather than a point. Our simulations indicate that the size of such a sheet would have to be at least on the order of the size of a convective cell in the helium shell. Whether detonation seeds of this kind are realistic can ultimately be answered only by suitable 3D convection simulations.

This research has been supported by the DOE SciDAC Program under contract DE-FC02-06ER41438; the National Science Foundation (AST 0909129) and the NASA Theory Program (NNX09AK36G). We acknowledge use-

ful discussions with Haitao Ma concerning the implementation of detonation physics in CASTRO. We also thank John Bell and Ann Almgren for their major roles in developing the CASTRO code. This research used resources of the National Energy Research Scientific Computing Center, which is supported by the Office of Science of the U.S. Department of Energy under Contract No. DE-AC02-05CH11231. This research used resources of the Oak Ridge Leadership Computing Facility at the Oak Ridge National Laboratory, which is supported by the Office of Science of the U.S. Department of Energy under Contract No. DE-AC05-00OR22725.

## REFERENCES

- Almgren, A. S., Beckner, V. E., Bell, J. B., Day, M. S., Howell, L. H., Joggerst, C. C., Lijewski, M. J., Nonaka, A., Singer, M., & Zingale, M. 2010, *ApJ*, 715, 1221
- Benz, W. 1997, in *NATO ASIC Proc. 486: Thermonuclear Supernovae*, ed. P. Ruiz-Lapuente, R. Canal, & J. Isern, 457
- Bildsten, L., Shen, K. J., Weinberg, N. N., & Nelemans, G. 2007, *ApJ*, 662, L95
- Dgani, R. & Livio, M. 1990, *ApJ*, 361, 540
- Fink, M., Hillebrandt, W., & Röpke, F. K. 2007, *A&A*, 476, 1133
- Fink, M., Röpke, F. K., Hillebrandt, W., Seitenzahl, I. R., Sim, S. A., & Kromer, M. 2010, *A&A*, 514, A53
- García-Senz, D., Bravo, E., & Woosley, S. E. 1999, *A&A*, 349, 177
- Livne, E. 1990, *ApJ*, 354, L53
- Livne, E. & Arnett, D. 1995, *ApJ*, 452, 62
- Livne, E. & Glasner, A. S. 1990, *ApJ*, 361, 244
- . 1991, *ApJ*, 370, 272
- Niemeyer, J. C. & Woosley, S. E. 1997, *ApJ*, 475, 740
- Röpke, F. K., Woosley, S. E., & Hillebrandt, W. 2007, *ApJ*, 660, 1344
- Seitenzahl, I. R., Meakin, C. A., Townsley, D. M., Lamb, D. Q., & Truran, J. W. 2009, *ApJ*, 696, 515
- Sim, S. A., Fink, M., Kromer, M., Röpke, F. K., Ruiter, A. J., & Hillebrandt, W. 2012, *MNRAS*, 420, 3003
- Taam, R. E. 1980, *ApJ*, 237, 142
- Timmes, F. X. & Arnett, D. 1999, *ApJS*, 125, 277
- Timmes, F. X., Hoffman, R. D., & Woosley, S. E. 2000, *ApJS*, 129, 377
- Timmes, F. X. & Swesty, F. D. 2000, *ApJS*, 126, 501
- Townsley, D. M., Moore, K., & Bildsten, L. 2012, *arXiv:1205.6517v1 [astro-ph.SR]*
- Weaver, T. A. & Woosley, S. E. 1978, *NASA STI/Recon Technical Report N*, 79, 32142
- Woosley, S. E. & Heger, A. 2007, *Phys. Rep.*, 442, 269
- Woosley, S. E., Heger, A., & Weaver, T. A. 2002, *Reviews of Modern Physics*, 74, 1015
- Woosley, S. E. & Kasen, D. 2011, *ApJ*, 734, 38
- Woosley, S. E. & Weaver, T. A. 1994, *ApJ*, 423, 371
- Zhang, W., Howell, L., Almgren, A., Burrows, A., & Bell, J. 2011, *ApJS*, 196, 20